Rail. Eng. Science (2022) 30(4):532–540
https://doi.org/10.1007/s40534-022-00284-z

Improved fault location method for AT traction power network based on EMU load test

Guosong Lin[1] · Xuguo Fu[1] · Wei Quan[1] · Bin Hong[1]

Received: 2 May 2022 / Revised: 30 June 2022 / Accepted: 3 July 2022 / Published online: 23 August 2022

Abstract The autotransformer (AT) neutral current ratio method is widely used for fault location in the AT traction power network. With the development of high-speed electrified railways, a large number of data show that the relation between the AT neutral current ratio and the distance from the beginning of the fault AT section to the fault point (Q–L relation) is mostly nonlinear. Therefore, the linear Q–L relation in the traditional fault location method always leads to large errors. To solve this problem, a large number of load-related current data that can be used to describe the Q–L relation are obtained through the load test of the electric multiple unit (EMU). Thus, an improved fault location method based on the back propagation (BP) neural network is proposed in this paper. On this basis, a comparison between the improved method and the traditional method shows that the maximum absolute error and the average absolute error of the improved method are 0.651 km and 0.334 km lower than those of the traditional method, respectively, which demonstrates that the improved method can effectively eliminate the influence of nonlinear factors and greatly improve the accuracy of fault location for the AT traction power network. Finally, combined with a short-circuit test, the accuracy of the improved method is verified.

✉ Guosong Lin
linguosong@swjtu.cn

Xuguo Fu
fuxuguo_98@163.com

Wei Quan
wquan@swjtu.edu.cn

Bin Hong
hongbin@my.swjtu.edu.cn

[1] School of Electrical Engineering, Southwest Jiaotong University, Chengdu 611756, China

Keywords Fault location · EMU load test · BP neural network · AT traction power network · High-speed electrified railway

1 Introduction

Fault location for the traction power network is an important guarantee for the safe and reliable operation of the traction power supply system. Common fault location methods for the traction power network include the reactance method, the autotransformer (AT) neutral current ratio method, the up-down-line current ratio method, the cross-line current ratio method, and so on [1–5]. Some scholars have studied the feasibility of the traveling wave method in fault location for the traction power network [6, 7]. However, compared with the transmission line in power systems, the catenary of one power supply section in the traction power network is too short, and a large number of branch lines and components are in parallel or in series with the network, so the traveling wave will be frequently refracted or reflected, which makes the wave head difficult to identify.

Faults in the AT traction power network are mainly short-circuit faults between the trolley line (T), the rail (R), and the negative feeder (F). The AT traction power network mainly adopts fault location methods based on the relation of the current ratio and the distance from the beginning of the fault AT section to the fault point [4], which can be applied to fault location under T to R short-circuit fault (T–R fault) or F to R short-circuit fault (F–R fault) of the AT traction power network with single-line, double-line, and cross-coupling AT power supply modes [8]. Among them, the cross-coupling AT power supply mode is the main mode of the AT traction power network in high-speed electrified railways. At present, some scholars have put forward some

improved methods and expansion schemes of fault location for the AT traction power network. In Refs. [9, 10], the impedance characteristics of the AT traction power network under short-circuit faults are studied by using the generalized symmetrical component method, which provides a theoretical basis for fault location. References [11, 12] proposed new schemes for identification of the section with the ground fault based on AT neutral currents, which is more accurate than the traditional identification method. Lin et al. [13] combined the AT neutral current ratio method and the reactance method to realize fault location for the over-zone feeding operation condition in high-speed electrified railways. Considering the structure of Korean railway system, Cho et al. [14] proposed a novel fault location method based on the relationship between AT neutral currents and branch currents, which improved the accuracy of fault location for Korean traction power supply system. Serrano et al. [15] proposed a method of ground fault location based on currents of the ATs. However, this method is sensitive to the fault current variations produced by the network voltage fluctuations or by the main transformer tap changer position. Therefore, in Ref. [16], Serrano improved the above method by replacing currents of ATs with the ratio of currents of ATs and substation transformer. However, this method is also based on the fault current distributions when a ground fault occurs, which is familiar with the traditional AT neutral current ratio method. In Ref. [17], a composite impedance model for general circuit topology of the AT section under different power supply modes is established. Based on this model, a unified fault location method suitable for various power supply modes and fault types is proposed, which is more accurate and robust.

In practical applications, due to the length of the AT section, the leakage reactance of the ATs, the leakage current on rails, and other factors, the traditional fault location method based on the Q–L relation needs to be corrected by the field short-circuit test or a small amount of historical short-circuit fault data [18–20]. However, this method has two main defects:

- Size of samples of the Q–L relation provided by the field short-circuit test or the historical short-circuit fault data is insufficient, which limits the correction ability of this method.
- With the increasing complexity of traction power supply system, the traditional fault location method cannot describe the nonlinear Q–L relation caused by a large number of influencing factors.

This paper introduces the electric multiple unit (EMU) load test and calculates the AT neutral current ratio through a large number of measured load-related current data obtained from the traction substation, the AT station, and the sectioning post that run the power supply arm, which provides a data basis for improving the traditional fault location method for the AT traction power network. References [21, 22] verify the feasibility of this scheme. The conclusions show that the distribution of locomotive load current in the traction power network can be equivalent to the distribution of short-circuit current, so as to obtain sample data that can be used to describe the Q–L relation. Aiming at the first defect of the traditional fault location method, some scholars combined with the load-related test data and established a linear regression model based on the least square method [23]. This method can be used to correct the parameters of the traditional fault location method, so as to improve the accuracy of fault location. However, it still cannot describe the nonlinear relation in the local area of the AT section. Therefore, in order to overcome the inherent defects of the traditional fault location method, an improved fault location method based on the BP neural network is proposed in this paper to describe the nonlinear Q–L relation in fact. The BP neural network has self-adaptive and self-learning ability, and its robustness and fault tolerance are strong. It is widely used in load forecasting, fault diagnosis, and other fields of power systems [24, 25].

2 Fault location method based on Q–L relation

When the T–R short-circuit fault occurs on the point f of the single-line AT traction power network, the AT neutral current distribution is shown in Fig. 1.

In Fig. 1, SS is the traction substation; ATP_n is the nth AT station in the AT power supply arm; T, R, and F are the trolley line, the rail, and the negative feeder, respectively; L is the distance from the beginning of the fault AT section to the fault point (in km); D is the length of the AT section where the fault is located (in km).

The AT neutral current ratio is defined as follow:

$$Q = \frac{I_{n+1}}{I_n + I_{n+1}}, \tag{1}$$

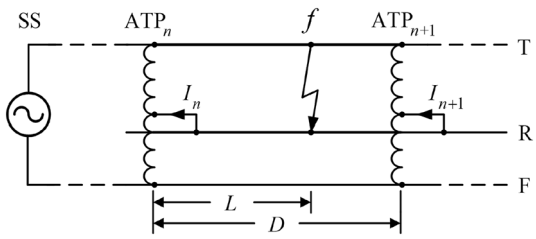

Fig. 1 Current distribution of load test of single-line AT traction power network

where I_n and I_{n+1} are values of AT neutral currents measured in the AT stations on both sides of the fault AT section (in A).

By analyzing the circuit shown in Fig. 1 and considering the practical application, the following correction equation for fault location can be obtained [4]:

$$L = \frac{Q - Q_1}{1 - (Q_1 + Q_2)} D, \tag{2}$$

where Q_1 and Q_2 are the parameters related to the length of AT section where the fault is located, the leakage reactance of ATs, the leakage current on rails, and other factors. AT sections of different railway lines have different values of Q_1 and Q_2. In practical applications, Q_1 and Q_2 in Eq. (2) are generally corrected by the short-circuit test data before the operation of electrified railways or the historical short-circuit fault data during the normal operation of electrified railways. The short-circuit test is destructive and it will impact the traction transformer, so it cannot be carried out in large quantities. Generally, each AT section only carries out short-circuit tests at one or two points for each fault type, which makes it still difficult to determine Q_1 and Q_2 in Eq. (2). No matter what correction method, Q and L reflect a linear relation in Eq. (2). However, in the practical application of fault location for AT traction power network in China's high-speed electrified railways, it is found that Q and L do not reflect the linear relation that is always mistaken by people, so the traditional fault location method based on Eq. (2) will still lead to errors to a certain extent.

3 EMU load test and data filtering

According to the characteristics of the AT traction power network, when a single-point ground fault or load operation occurs at the same position, the same AT neutral current ratio can be obtained. The value is determined by the position of ground fault or load and system parameters of AT traction power network, which is basically independent of the absolute value and phase difference of current.

The fault location system can only locate the single-point fault in AT section, so only one EMU is used for the load test. When there are multiple loads, the test data are invalid. As shown in Fig. 2, the EMU load test system includes current sampling devices with synchronous clocks and a position recorder. In Fig. 2, SP is the sectioning post. In the test, the load of one EMU simulates the T–R fault to realize the effect of multiple short-circuit tests at different positions of the test section. By recording AT neutral currents at SS, ATP, and SP and the relation between the position of the EMU and time on the EMU, the EMU load data that simulate the T–R fault can be collected to describe the Q–L relation [22].

During the test, the current sampling devices collect the effective values of the AT neutral current ratio at SS, ATP, and SP on the same power supply arm at an interval time of 1 s. The position recorder records the kilometer post of the EMU in real time.

Due to the influence of system errors such as the accuracy of the current transformer, the accuracy of current sampling devices, and synchronization of clocks at each station, there are some abnormal data with the unreasonable Q–L relation; so it is necessary to set reasonable filtering methods. In this paper, the validity of data is verified based on the Kirchhoff theorem on the whole power supply arm composed of the traction substation, the AT station, and the sectioning post. For example, the current distribution is shown in Fig. 3 when the EMU load test is carried out on the cross-coupling AT traction power network.

In Fig. 3, $\dot{I}_{T1}$, $\dot{I}_{F1}$, $\dot{I}_{T2}$, and $\dot{I}_{F2}$ are the current in the down-line trolley line, the current in the down-line feeder, the current in the up-line trolley line, and the current in the up-line feeder, respectively (in A); $\dot{I}_1$ and $\dot{I}_2$ are AT neutral currents of AT_1 and AT_2, respectively (in A).

Generally, the sum of effective values of the four feeder currents in the traction substation is approximately equal to the sum of effective values of AT neutral currents of the transformers in the traction substation, the AT station, and

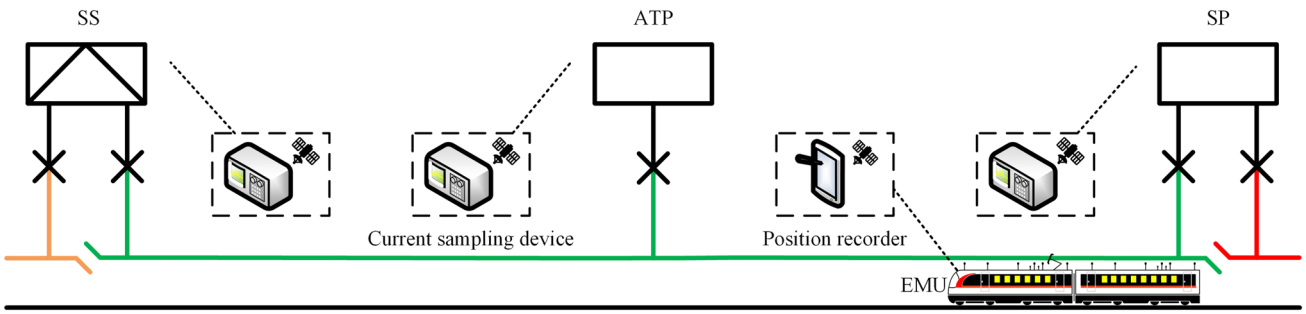

Fig. 2 Schematic diagram of EMU load test system

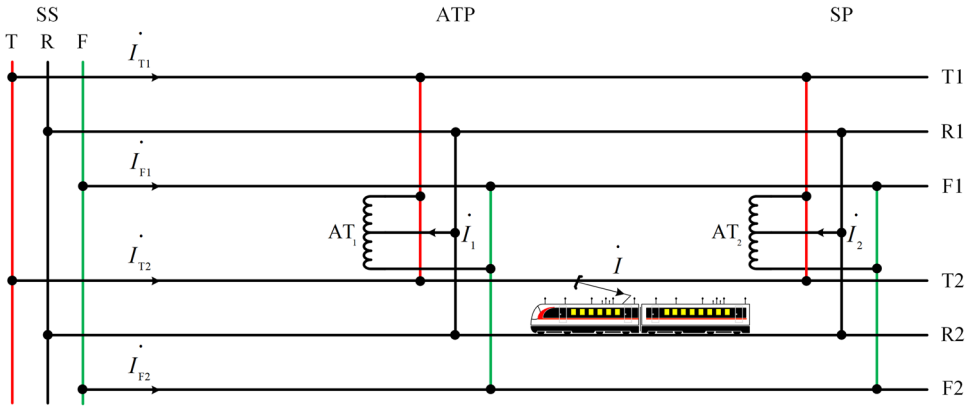

Fig. 3 Current distribution of Load test of cross-coupling AT traction power network

the sectioning post [4]. Therefore, one of the data filtering principles can be expressed as

$$I_{T1} + I_{F1} + I_{T2} + I_{F2} - I_s - I_1 - I_2 \geq I_{set1}, \tag{3}$$

where I_s is AT neutral current of the transformer in the traction substation (in A), $I_s = |\dot{I}_{T1} + \dot{I}_{F1} + \dot{I}_{T2} + \dot{I}_{F2}|$ [4]; I_{set1} is generally considered according to the maximum unbalanced current caused by system errors. In engineering, the setting value of I_{set1} can be adjusted in combination with the actual collected data. When this condition is met, the data point is invalid.

At the same time, based on the principle that the sum of the effective values of the four feeder currents in the traction substation is approximately equal to the load current of the EMU, the load current of the EMU can be estimated, and the data collected when the load current of the EMU is low can be discarded to avoid the influence of system errors. Therefore, another data filtering principle can be expressed as

$$I_{T1} + I_{F1} + I_{T2} + I_{F2} \leq I_{set2}, \tag{4}$$

where I_{set2} is the minimum allowable load current of the EMU (in A), it is generally considered according to the low load current when the EMU runs slowly or is stopped. When this condition is met, the data point is invalid.

It should be noted that the characteristic with the Q–L relation corresponding to the F–R fault is different from that of the T–R fault, so the above load test based on the EMU is not feasible. However, based on the same theory, the Q–L relation corresponding to the F-R fault can be obtained by using movable impedance. The movable impedance can be a resistance or capacitor with enough capacity, which is installed on the rail flat car. The two ends of the movable impedance are, respectively, connected with the negative feeder and the rail. At different positions, the F–R fault test can be realized.

4 Improved fault location method based on BP neural network

In order to establish a model to describe the nonlinear Q–L relation according to the data of the EMU load test and realize fault location, the nonlinear regression method based on the back propagation (BP) neural network is adopted in this paper. The BP neural network is a feedforward neural network based on the error back propagation algorithm, which has the ability to deal with linear inseparable problems. The BP neural network includes the input layer, the hidden layer, and the output layer. The universal approximation theorem shows that multilayer feedforward neural network can approximate continuous functions of arbitrary complexity with arbitrary accuracy with only one hidden layer containing enough neurons [26]. The BP neural network topology established in this paper is shown in Fig. 4.

In this model, the input layer and the output layer are the AT neutral current ratio Q and the distance L, respectively. The setting of the number of neurons in the hidden layer is an open problem. The range is usually determined by the empirical formula and adjusted by the trial and error method [26]. The number of neurons in the hidden layer can be determined as follows [27]:

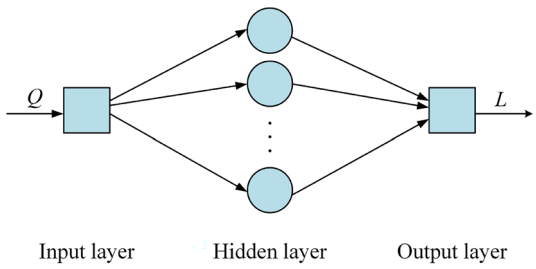

Fig. 4 Neural network topology

$$p = \sqrt{m+n} + a, \tag{5}$$

where p, m, and n are the number of neurons in the hidden layer, the input layer, and the output layer, respectively; a is a constant in the range of [0, 10].

In this paper, the Tansig function and the Purelin function are used as the transfer functions of the hidden layer and the output layer, respectively. The expressions of Tansig function and Purelin function are shown in Eqs. (6) and (7), respectively [28]:

$$g(x) = \frac{2}{1+\mathrm{e}^{-2x}} - 1, \tag{6}$$

$$g(x) = x. \tag{7}$$

In this paper, the mean square error is used as the loss function, and the expression is shown as follows:

$$\mathrm{MSE} = \frac{1}{n}\sum_{i=1}^{n}\left(y_i - \hat{y}_i\right)^2, \tag{8}$$

where y_i is the true value of the output of the sample; $\hat{y}_i$ is the output of the neural network.

In order to optimize the gradient descent method, the learning algorithm in this paper adopts the Levenberg–Marquardt optimization algorithm and this algorithm has an excellent performance in training time, iteration times, and training errors [29, 30].

In order to improve the training speed, the samples should be normalized to −1 to 1 according to the following equation before training:

$$x^* = \frac{2\left(x - x_{\min}\right)}{x_{\max} - x_{\min}} - 1, \tag{9}$$

where x is the original samples; x^* is normalized results of the original samples; $x_{\max}$ and $x_{\min}$ are the maximum and the minimum values in the original samples, respectively.

The fault location equation based on the BP neural network can be expressed as

$$L^* = \mathrm{purelin}((\boldsymbol{\omega}^{(2)})^{\mathrm{T}} \cdot \mathrm{tansig}(\boldsymbol{\omega}^{(1)} \cdot Q^* + \boldsymbol{b}^{(1)}) + b^{(2)}), \tag{10}$$

where $\boldsymbol{\omega}^{(i)}$ is the weight of the ith layer; $\boldsymbol{b}^{(i)}$ is the threshold of the ith layer; L^* is normalized result of the distance from the beginning of the AT section where the fault is located to the fault point; Q^* is normalized result of the AT neutral current ratio.

After the calculation, in order to obtain the final actual fault distance, the normalized result should be denormalized according to the following equation:

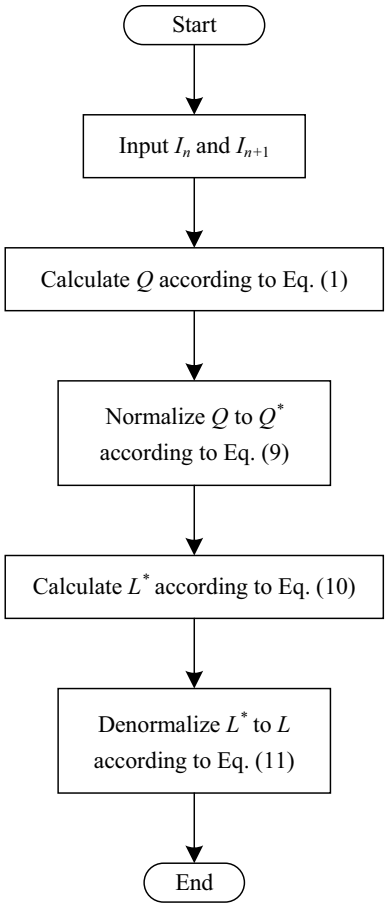

Fig. 5 Flowchart of the improved fault location method

$$L = \frac{(L^*+1)\cdot\left(L_{\max} - L_{\min}\right)}{2} + L_{\min}, \tag{11}$$

where $L_{\max}$ and $L_{\min}$ are the maximum and the minimum values of samples of fault distances, respectively (in km).

The flowchart of the improved fault location method is shown in Fig. 5.

5 Verification and comparison

5.1 Data processing

The EMU load test was carried out on the up line of the ATP-SP section in Meizhou–Shantou high-speed railway in Guangdong, China. The kilometer posts of the AT station and the sectioning post are 54.103 km and 38.581 km, respectively. The variables collected during the test are shown in Table 1. Based on the data of the EMU load test, the Q–L relation samples for the corresponding AT section can be calculated according to Eq. 1. During the operation of EMU, the load current is about 200 A to 400 A. Therefore,

when I_{set1} and I_{set2} in Eqs. (3) and (4) were set to 20 A and 100 A, respectively, the data of the EMU load test that may cause large errors can be filtered to improve the effectiveness of the Q–L relation samples. The complete data samples contain 571 data points, including 405 valid data points and 166 invalid data points. In order to verify the effectiveness of the improved fault location method, the Q–L relation samples can be divided into group A and group B according to the parity characteristics in the order of distance coordinates, so as to ensure the uniformity of sample distribution in the AT section. Group A and group B of the Q–L relation samples are shown in Fig. 6.

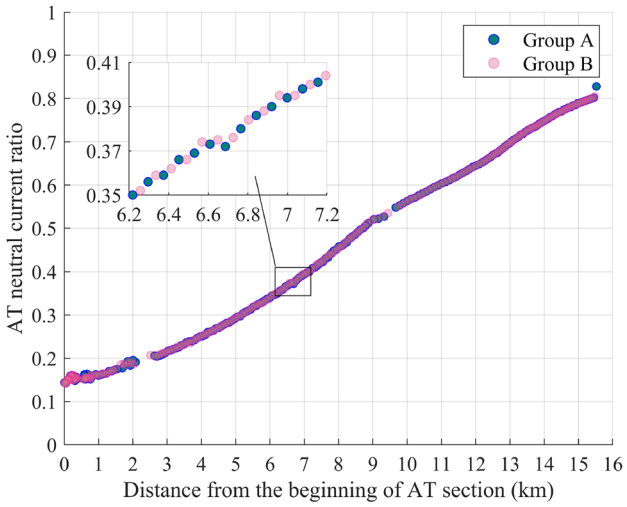

Fig. 6 Grouping diagram of Q–L relation samples

5.2 Effectiveness verification of different methods

In order to obtain the parameters of the improved fault location method and the traditional fault location method, the BP neural network and the linear least square method were, respectively, used to realize the regression of the Q–L relation samples in group A. Based on MATLAB, these two models were built. In the training process of the BP neural network, the train set, the validation set, and the test set are 70%, 15%, and 15% of the random Q–L relation samples in group A, respectively. In this paper, the learning rate is 0.001, the maximum number of iterations is 1000, the expected error is 5×10^{-4}, and the maximum number of validation is 6. According to Eq. (5), the empirical range of the number of neurons in the hidden layer can be 2–12. After many tests, the performance of the model is basically unchanged when there are more than three neurons in the hidden layer, as shown in Table 2. Among them, the model parameters are determined by the training of group A of the Q–L relation samples, and the average absolute errors are obtained by the test of group B of the Q–L relation samples. To decrease the complexity and increase training and calculation speed of the model, the number of neurons in the hidden layer should be 4.

The variation curves of the mean square errors of each dataset are shown in Fig. 7. During 125 iterations of training, the mean square error of the validation set could not decrease for 6 consecutive times. The mean square error of the validation set is 6.528×10^{-3}, which is shown in Fig. 7. The regression of the Q–L relation based on the BP neural network and the least square method is shown in Fig. 8. By comparing with the regression of the least square method, it can be concluded that the BP neural network can more effectively describe the Q–L relation with the T–R fault.

The parameters obtained based on the two regression methods are shown in Table 3. In this table, Q_1 and Q_2 in the traditional fault location method are parameters related to AT neutral currents corresponding to the distance coordinate of the regression result using the least square method at the beginning and the end of the AT section.

In order to further verify the superiority of the improved fault location method, it is necessary to compare the accuracy of the two fault location methods through the data which are not involved in the regression of the Q–L relation

Table 1 Variables contained in the dataset

Variable	Collection place
$\dot{I}_{T1}$	Traction substation
$\dot{I}_{F1}$	Traction substation
$\dot{I}_{T2}$	Traction substation
$\dot{I}_{F2}$	Traction substation
$\dot{I}_1$	AT station
$\dot{I}_2$	Sectioning post
Kilometer post	EMU

Table 2 Errors of neural network with different numbers of neurons in hidden layer

Number of neurons	Average absolute error (km)
2	0.100
3	0.100
4	0.065
5	0.066
6	0.065
7	0.061
8	0.063
9	0.068
10	0.060
11	0.062
12	0.061

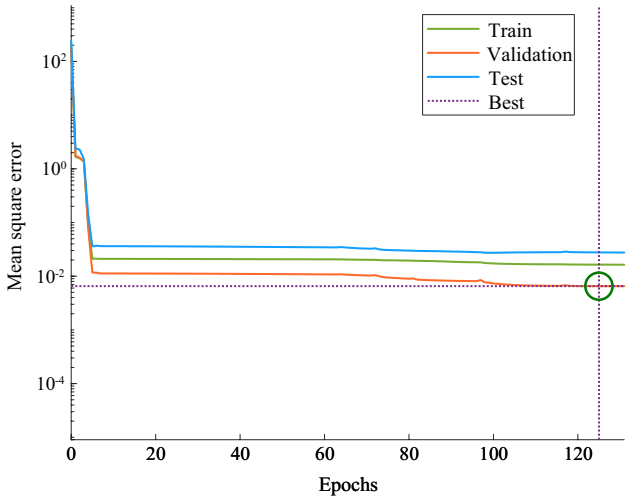

Fig. 7 Training performance

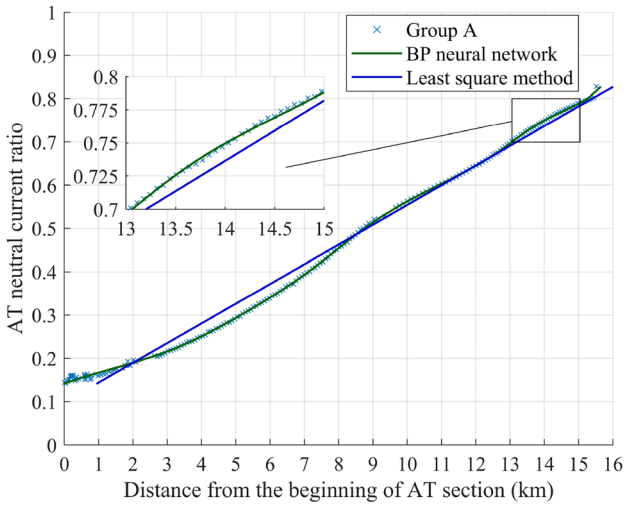

Fig. 8 Regression of Q–L relation based on two methods

Table 3 Parameter values of two methods

Method	Parameter	Value
Improved method	$\boldsymbol{\omega}^{(1)}$	$(7.3615, -3.0357, -1.7491, -6.7746)^{\mathrm{T}}$
	$\boldsymbol{\omega}^{(2)}$	$(0.1316, -0.3214, -0.5300, -0.1899)^{\mathrm{T}}$
	$\boldsymbol{b}^{(1)}$	$(-6.2014, 1.0933, -1.0216, -6.1875)^{\mathrm{T}}$
	$b^{(2)}$	−0.1163
	$L_{\max}$	15.5220
	$L_{\min}$	0.0000
	$Q_{\max}$	0.8280
	$Q_{\min}$	0.1420
Traditional method	Q_1	0.0985
	Q_2	0.1970

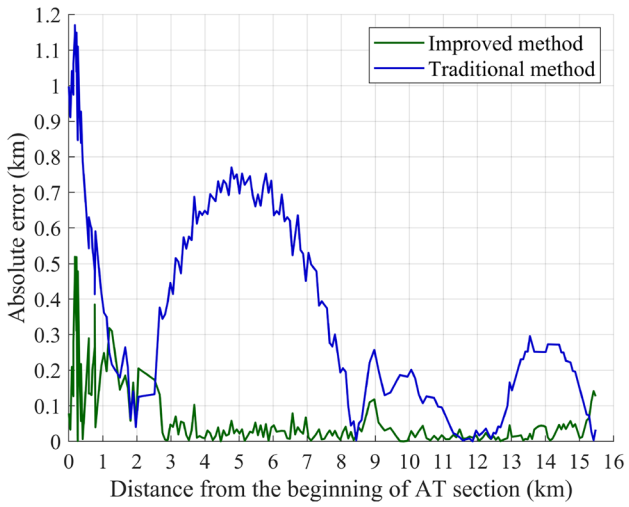

Fig. 9 Absolute errors of two fault location methods

according to the parameters shown in Table 3. Therefore, group B of the Q–L relation samples is used to compare the fault location capabilities of the improved fault location method and the traditional fault location method in the whole section where the fault is located. The absolute error is used in this paper to evaluate two fault location methods. Absolute errors of fault location results of two fault location methods are shown in Fig. 9. It can be concluded that the maximum absolute error and the average absolute error of the fault location results of the traditional fault location method are 1.170 km and 0.399 km, while the maximum absolute error and the average absolute error of the fault location result of the improved fault location method are only 0.519 km and 0.065 km, which show that the performance of the improved fault location method is better than that of the traditional fault location method in the local and the whole area of the fault AT section.

5.3 Verification by short-circuit test

Before the formal opening of the Meizhou–Shantou high-speed railway, several short-circuit tests with different fault types and different locations were carried out. The data of a T–R short-circuit test are shown in Table 4.

Based on the parameters of the improved fault location method suitable for the fault AT section shown in Table 3, the accuracy of the proposed method in practical applications is verified. According to Eqs. (1), (9)–(11), and parameters shown in Eq. (3), the length of the fault given by Eq. (4) is 15.480 km and the error is only 0.008 km, while the error of the traditional method is 0.221 km.

Table 4 Fault information of T–R short-circuit test in Meizhou–Shantou high-speed railway

Position	Kilometer post (km)	AT neutral current (A)
AT station	54.103	1009.37
Sectioning post	38.581	4004.36
Fault	38.631	–

6 Conclusion

In this paper, to improve the accuracy of fault location for the AT traction power network in high-speed electrified railways, the EMU load test is introduced. Using the current data of the EMU load test, the regression method based on the BP neural network is applied, and an improved fault location method is proposed. Compared with the traditional fault location method, the maximum absolute error and the average absolute error of the improved fault location method are significantly lower. The application based on the short-circuit test data also shows that the method has high accuracy and can effectively eliminate the adverse impact of the nonlinear Q–L relation on fault location for the AT traction power network in high-speed electrified railways.

It is worth pointing out that the BP neural network applied by the improved method has a small parameter scale, simple training method, fast operation speed, and high prediction efficiency, so it is easy to be applied in engineering.

Acknowledgements This work was supported by the National Key Research and Development Program of China (No. 2021YFB2601500) and the Natural Science Foundation of Sichuan Province (No. 2022NSFSC0405).

References

1. Zhou Y, Xu G, Chen Y (2012) Fault location in power electrical traction line system. Energies 5(12):5002–5018
2. Xu G, Zhou Y, Chen Y (2013) Model-based fault location with frequency domain for power traction system. Energies 6(7):3097–3114
3. Han Z, Li S, Liu S, Gao S (2020) A reactance-based fault location method for overhead lines of ac electrified railway. IEEE Trans Power Deliv 35(5):2558–2560
4. Lin G (2010) Study on novel protection and location schemes for traction power supply system. Dissertation, Southwest Jiaotong University (in Chinese)
5. Guo M, Lin G, Chen X (2006) Fault locator of all-paralleling at traction power supply based on the theory of the current ratio of paralleling lines. Relay 34(22):36–39 (in Chinese)
6. Xiong L, Wu G, Wang Z (2019) Study on fault location of multi measuring points traveling wave method based on IHHT in all parallel AT traction network. Trans China Electrotech Soc 34(15):3244–3252 (in Chinese)
7. Jiao Z, Gao S (2003) Study on the feasibility of using traveling wave in the fault location in the overhead contact network of electrified railway traction. Relay 31(7):33–36 (in Chinese)
8. Lu T, Han Z, Wang J (2006) Fault location method for all-parallel autotransformer feeding systems. Proc CSU-EPSA 18(2):27–30 (in Chinese)
9. Lin G, Li Q (2010) Impedance calculations for AT power traction networks with parallel connections. In: 2010 Asia-Pacific Power and Energy Engineering Conference, Chengdu
10. Li G, Lin G (2012) Short circuit impedance analysis for novel AT power traction network. In: 2012 Asia-Pacific Power and Energy Engineering Conference, Chengdu
11. Wang C, Yin X (2012) Comprehensive revisions on fault-location algorithm suitable for dedicated passenger line of high-speed electrified railway. IEEE Trans Power Deliv 27(4):2415–2417
12. Serrano J, Platero CA, López-Toledo M, Granizo R (2015) A novel ground fault identification method for 2 × 5 kv railway power supply systems. Energies 8(7):7020–7039
13. Lin G, Quan W, Tong X (2021) Fault location scheme for over-zone feeding operation condition on high-speed railway. J Electr Eng Technol 17:1459–1467
14. Cho G-J, Kim C-H, Kim M-S, Kim D-H, Heo S-H, Kim H-D, Min M-H, An T-P (2019) A novel fault-location algorithm for ac parallel autotransformer feeding system. IEEE Trans Power Deliv 34(2):475–485
15. Serrano J, Platero C, López-Toledo M, Granizo R (2017) A new method of ground fault location in 2 × 25 kV railway power supply systems. Energies 10(3):340
16. Platero CA, Serrano J, Guerrero JM, Fernández-Horcajuelo A (2021) Ground fault location in 2 × 25 kV high-speed train power systems by (auto)transformers currents ratio. IEEE Trans Power Deliv 36(5):3065–3073
17. Wang S, Chen M, Li Q, Kou Z (2021) A unified fault-location method of autotransformer traction network for high-speed railway. IEEE Trans Power Deliv 36(6):3925–3936
18. Chou C-J, Hsiao Y-T, Hsu C-C et al (2001) Distribution of earth leakage currents in railway systems with drain auto-transformers. IEEE Trans Power Deliv 16(2):271–275
19. Chou C-J, Hsiao Y-T, Hsu C-C et al (1999) Distribution of earth leakage currents in railway systems with drain auto-transformers. In: 1999 IEEE Transmission and Distribution Conference, New Orleans
20. Wang J (2006) Research on fault location of all-parallel at traction system. Dissertation, Southwest Jiaotong University (in Chinese)
21. Yu G (2014) Check distance measurement accuracy of at suck current ratio with locomotive load current. J Railw Eng Soc 31(7):95–98 (in Chinese)
22. Miu B, Li R, Ai G (2019) Research and modification on fault location method for traction power supply system in high speed railway. Electr Railw 30(1):20–23 (in Chinese)
23. Mohanpurkar M, Suryanarayanan S (2014) Regression modeling for accommodating unscheduled flows in electric grids. IEEE Trans Power Syst 29(5):2569–2570

24. He Z, Gao S, Chen X, Zhang J, Bo Z, Qian Q (2011) Study of a new method for power system transients classification based on wavelet entropy and neural network. Int J Electr Power Energy Syst 33(3):402–410
25. Chen B, Wang Y (2021) Short-term electric load forecasting of integrated energy system considering nonlinear synergy between different loads. IEEE Access 9:43562–43573
26. Zhou Z (2016) Machine learning. Tsinghua University Press, Beijing (in Chinese)
27. Yao Z, Pan F, Shen Y, Wu J, Yu X (2015) Short-term prediction of photovoltaic power generation output based on GA-BP and POS-BP neural network. Power Syst Prot Control 43(20):83–89 (in Chinese)
28. Chen M (2013) Principles and examples of MATLAB neural network. Tsinghua University Press, Beijing (in Chinese)
29. Yan Z, Fan X, Zhao W, Xu X, Fan J, Wang Y (2015) Improving the convergence of power flow calculation by a self-adaptive Levenberg–Marquardt method. Proc CSEE 35(8):1909–1918 (in Chinese)
30. Wang Y, Wu C, Zhou D, Li Z et al (2013) A survey of fault diagnosis for PV array based on BP neural network. Power Syst Prot Control 41(16):108–114 (in Chinese)